Available online at www.sciencedirect.com
SCIENCE DIRECT®
Journal of Nuclear Materials 335 (2004) 397–409
journal of nuclear materials
www.elsevier.com/locate/jnucmat

Synthesis and characterization of low-temperature precursors of thorium–uranium (IV) phosphate–diphosphate solid solutions

N. Clavier [a], N. Dacheux [a,*], P. Martinez [a], V. Brandel [a], R. Podor [b], P. Le Coustumer [c]

[a] *Groupe de Radiochimie, Institut de Physique Nucléaire d'Orsay, Université Paris-Sud-11, Bât. 100, 91406 Orsay, France*
[b] *LCSM, Université H. Poincaré – Nancy I, BP 239, 54506 Vandoeuvre lès Nancy, France*
[c] *CDGA, Université de Bordeaux I, BP 19, Avenue des facultés, 33405 Talence, France*

Received 4 June 2004; accepted 23 July 2004

Abstract

Several compositions of new precursor of thorium–uranium (IV) phosphate–diphosphate solid solutions ($Th_{4-x}U_x(PO_4)_4P_2O_7$, called β-TUPD) were synthesized in closed PTFE containers either in autoclave (160 °C) or on sand bath (90–160 °C). All the samples appeared to be single phase. From XRD data and TEM observations, the diffraction lines matched well with that of pure thorium phosphate–hydrogenphosphate hydrate (TPHPH), $Th_2(PO_4)_2(HPO_4)\cdot H_2O$, which confirmed the preparation of a complete solid solution between pure thorium and uranium (IV) compounds. TGA/DTA experiments showed that samples of thorium–uranium (IV) phosphate–hydrogenphosphate hydrate (TUPHPH) prepared at 150–160 °C were monohydrated leading to the proposed formula $Th_{2-x/2}U_{x/2}(PO_4)_2(HPO_4)\cdot H_2O$. The variation of the XRD diagrams versus the heating temperature showed that TUPHPH remained crystallized and single phase from room temperature to 200 °C. After heating between 200 °C and 800 °C, the presence of diphosphate groups in the solid was evidenced. In this range of temperature, the solid was transformed into the low-temperature monoclinic form of thorium–uranium (IV) phosphate–diphosphate (α-TUPD). This latter compound finally turned into well-crystallized, homogeneous and single-phase β-TUPD (orthorhombic form) above 930–950 °C for x values lower than 2.80. For higher x values, a mixture of β-TUPD, α-$Th_{1-z}U_zP_2O_7$ and $U_{2-w}Th_wO(PO_4)_2$ was obtained. By this new chemical route of preparation of β-TUPD solid solutions, the homogeneity of the samples is significantly improved, especially considering the distribution of thorium and uranium.

1. Introduction

In order to proceed to the immobilization of radioactive waste, the most likely option considered consists in an underground repository. One of the main problems for this kind of conditioning is the infiltration of

* Corresponding author. Tel.: +33 1 69 15 73 46; fax: +33 1 69 15 71 50.
E-mail address: dacheux@ipno.in2p3.fr (N. Dacheux).

0022-3115/$ - see front matter © 2004 Elsevier B.V. All rights reserved.
doi:10.1016/j.jnucmat.2004.07.048

groundwater which could induce the release of radionuclides then their migration to the biosphere. Among the radionuclides to be stored, actinides must be considered carefully due to their long-term high radiotoxicity and to their long half-life period. Several phosphate-based materials such as apatites ($Ca_{10}(PO_4)_6F_2$) and associated britholites ($Ca_9Nd(PO_4)_5(SiO_4)F_2$) [1,2], monazites ($LnPO_4$) and associated brabantites ($M^{II}M^{IV}(PO_4)_2$) [3–9], sodium dizirconium phosphate ($NaZr_2(PO_4)_3$, NZP) [10–13] or uranium and thorium phosphates [14–21] were studied as potential matrices to stabilize these radionuclides in solids (e.g. ceramics). Several properties including an easy way of preparation, a good behavior during sintering and a strong resistance to aqueous corrosion were especially considered and required.

β-TPD appears as a promising material for the immobilization of tetravalent actinides [14,22,24]. Actually, it was demonstrated that β-TPD can incorporate large amounts of tetravalent uranium (up to 47.6 wt%), neptunium (33.2 wt%) or plutonium (26.1 wt%) by substitution of thorium [17–20,23]. The synthesis of such solids was performed following several ways including either wet or dry chemistry routes. Sintered pellets were prepared using a two-step procedure (involving an uniaxial pressing at room temperature followed by a heat treatment at 1250 °C). For all the samples, the apparent and effective relative densities reached 90–95% and 94–99% of the value calculated from XRD data, respectively [24]. Leaching tests achieved in various solutions demonstrated that both powdered and sintered samples doped, or not, with tetravalent actinides, exhibit a strong resistance to aqueous corrosion [21,25,26]. The normalized dissolution rate ranges from $(5.8 \pm 0.3) \times 10^{-6}\,g\,m^{-2}\,day^{-1}$ (10^{-1} M HNO_3) to $(4.8 \pm 0.3) \times 10^{-8}\,g\,m^{-2}\,day^{-1}$ (pH = 7) at room temperature, which is several orders of magnitude lower than for other matrices such as basaltic glasses [27]. The dissolution of β-TPD is rapidly followed by the formation of neoformed phases containing radionuclides in the back-end of the dissolution of the initial ceramic: they are thorium phosphate–hydrogenphosphate hydrate $Th_2(PO_4)_2(HPO_4).H_2O$ (TPHPH) for thorium [28] and uranyl phosphate pentahydrate for uranium (tetravalent uranium being oxidized into uranyl during the dissolution process) [21,26]. Due to the different chemical behaviors of thorium and uranium during leaching tests, the heterogeneity of the samples can degrade their chemical durability through the presence of U-enriched secondary phases. For this reason, we tried to improve the chemical homogeneity of thorium–uranium (IV) phosphate–diphosphate solid solutions (β-TUPD) and especially the distribution of the actinides in the final material through their preparation from $Th_{2-x/2}U_{x/2}(PO_4)_2(HPO_4) \cdot H_2O$ (TUPHPH solid solutions). In this aim, these precursors as well as the chemical reactions leading to their transformation into the final β-TUPD samples, were followed using several techniques of characterization.

2. Experimental

2.1. Synthesis

Concentrated thorium chloride solutions ($C \approx 1.8$ M) were issued from Rhodia (France). Uranium chloride solution was obtained from the dissolution of uranium metal chips in 4 M HCl. The initial solutions were diluted in order to obtain a final concentration of 0.7 M for thorium and 1.1 M for tetravalent uranium. The other chemical reagents of 'pro-analysis' grade used for syntheses and for analyses were from Aldrich, Fluka and VWR. The concentrations of the final solutions were determined using conventional analytical methods.

The precipitation of solid solutions followed two methods, both involving a mixture of concentrated solutions of the cations and of 5 M H_3PO_4 in PTFE containers. For the first kind of syntheses, the closed container was put on a sand bath ($\theta = 150$ °C) for several hours to four weeks. For hydrothermal syntheses, PTFE containers were placed in autoclaves supplied by Parr Instrument Company. This system was set in an oven at 160 °C for about one month. The crystallized solids prepared by both ways were then separated from the liquid phase by filtration or centrifugation (at 3000 rpm), washed several times with deionized water in order to eliminate the remaining acid and finally dried.

2.2. Characterization

Heat treatments were performed in alumina boats in PYROX MDB 15 or HM 40 furnace up to 1250 °C with heating rates of 2–5 °C min^{-1}. In order to prevent the oxidation of uranium (IV) into uranyl, all the heating treatments were performed under argon atmosphere.

The XRD diagrams were collected with a Philips X'PERT-PRO – PW 3040/60 or Brüker D8 Advanced Roentgen diffractometer system using Cu Kα rays ($\lambda = 1.5418$ Å). The precise peaks positions were determined using the fitting program EVA, available in the software package Diffrac-AT V 3.0 [29]. Diagrams were recorded from room temperature to 1100 °C under N_2 atmosphere using a HTK 1200 furnace from Anton Parr Instrument Company. Infrared absorption spectra were recorded from 400 to 4000 cm^{-1}, using cylindrical pellets ($\varnothing = 10$ mm) of about 1 wt% of powder in KBr, with an Hitachi I-2001 spectrophotometer. HT-Raman absorption spectra were collected from room temperature to 300 °C by means of a Dilor–Jobin Yvon apparatus using a Ar-laser working at 514.5 nm. The power varied from

50 to 100 mW and the laser beam was focused on the sample with an Olympus microscope. TGA and DTA experiments were done using a Setaram TG 92-16 apparatus, in alumina crucibles, under argon atmosphere with heating rates of 2–5 °C min^{-1} and cooling rate of 20 °C min^{-1}.

Electron probe microanalyses (EPMA) were carried out using a Cameca SX 50 apparatus with an acceleration voltage of 15 kV and a current of 10 nA considering the following calibration standards: $SmPO_4$ (K_α ray of phosphorus), ThO_2 (M_α ray of thorium) and UO_2 (M_β ray of uranium). The counting time was fixed to 10–30 s while the size of the spot was 1 μm. PIXE analyses were performed with a Tandem-type accelerator using a 3 MeV proton beam and using β-TPD, $U(UO_2)(PO_4)_2$, α-UP_2O_7 and $U_2O(PO_4)_2$ as external monitors.

SEM micrographs were collected using a Hitachi S2500 scanning electron microscope. TEM observations were carried out using either a Philips CM12 or a CM30 apparatus. Both are equipped with high resolution stage with spatial resolution (point to point) of 0.22 nm for the CM12 and 0.18 nm for the CM30. The use of high resolution (HR) mode allows to determine texture at the nanometric scale and reveals the organization of atomic planes. The bright field (BF) mode reveals texture at the submicrometric scale. Coupled with dark field (DF) mode, it allows the observation of structural details such as amorphous or crystallized domains. In fact, DF was used for two perpendicular positions (0° and 90°) of the diffracted beam selected. If diffracted domains appear bright for one position and dark for the second one, the material is thus crystallized. On the contrary, if the domains appear slightly illuminated for both positions, the material can be considered amorphous or poorly crystallized. Selected area diffraction (SAD) leads to structural determination (single crystal, polycrystalline material or amorphous one) at the micrometric scale. In fact, the area selected with a parallel beam is estimated to 5–10 μm^2.

3. Results and discussion

3.1. Characterization of the solid

3.1.1. PIXE and EPMA experiments

The homogeneity and the chemical composition of all the solid prepared were checked by particle induced X-ray emission (PIXE) and electron probe micro-analyses (EPMA). The results obtained are gathered in Table 1 and compared to that of thorium phosphate–hydrogenphosphate hydrate (TPHPH). The representation of the data obtained in the ternary system ThO_2–UO_2–P_2O_5 (wt%) is given in Fig. 1. For each sample, the composition is consistent with that calculated from the global formulae. The initial excess of phosphoric acid used during the synthesis does not have any influence on the stoichiometry of the final compound in which the mole ratio $(U + Th)/PO_4$ remained invariably equal to 2/3. The stoichiometry was also verified in the pure TPHPH and in the end-member of the series: UPHPH. However, in several samples, the U/(Th + U) mole ratios were slightly lower than expected probably due to the partial oxidation of uranium (IV) into uranyl during the precipitation process (up to 5–10 mol%). More generally, all the samples prepared appeared homogeneous and single phase with a significant improvement of the cationic distribution (Th, U) in the powdered precursors compared to that already studied up to present (through dry chemical routes or via direct evaporation of the initial mixture) as it will be evidenced in the following sections for a given β-TUPD solid solution.

3.1.2. XRD study

In order to verify the existence of TUPHPH solid solutions, XRD diagrams were recorded for several chemical compositions (Fig. 2). The unit cell parameters were refined by the means of U-Fit program [30] considering the space group $P2_1$ [31]. For each compound, all the diffraction lines observed are consistent with that previously reported for TPHPH [22,28,31]. No additional diffraction line was found which confirmed that the samples were all single phase. Nevertheless, some weak differences were observed in the I/I_0 relative intensities due to the powder morphology suggesting the preferential orientation of the grains in the sample (2D structure built from the (0 0 l) planes) [22]. The set of unit cell parameters is gathered in Table 2. The variation of the unit cell parameters and volume versus the thorium substitution rate are gathered in Table 3 and plotted in Fig. 3. The linear decrease of the unit cell parameters confirmed the progressive replacement of thorium ($^{VII}r_{Th}$ = 1.00 Å) by the smaller uranium (IV) ($^{VII}r_U$ = 0.95 Å) in the structure and, by the way, the existence of a complete solid solution between both end-members TPHPH and UPHPH. However, the unit cell parameters are only weakly affected when replacing thorium by uranium (IV): the relative decrease of the unit cell parameters is only 1.3, 1.0 and 1.3% along the a, b and c axis, respectively, while the β angle remains almost constant (107.30° to 107.40°). These variations correspond to a volume drop of about 3.6%.

3.1.3. Scanning electron microscopy (SEM)

Micrographs of precursor are presented in Fig. 4 for two chemical compositions: $x = 0.4$ (Fig. 4(a)–(c)) and $x = 3.2$ (Fig. 4(d)–(f)). The crystal size is about 2–5 μm for both compositions. The crystal morphology of the small plates (Fig. 4(b) and (c)) is consistent with preferential orientations suggested from X-ray diffraction patterns. Some large aggregates (10–15 μm) are observed in several micrographies (Fig. 4(a) and (d)) and

Table 1
Results of EPMA and PIXE experiments for various compositions of TUPHPH solid solutions

Sample	Th/wt%	U/wt%	P/wt%	(U + Th)/P	U/(Th + U)
$Th_2(PO_4)_2(HPO_4)\cdot H_2O$					
Calc.	60.4	0	12.1	0.67	0
PIXE	64.3 ± 3.1	–	12.4 ± 0.6	0.69 ± 0.04	–
EPMA	60.4 ± 0.5	–	12.4 ± 0.1	0.65 ± 0.01	–
$Th_{1.9}U_{0.1}(PO_4)_2(HPO_4)\cdot H_2O$					
Calc.	57.4	3.1	12.1	0.67	0.05
PIXE	60.5 ± 3.0	2.5 ± 0.1	12.3 ± 0.6	0.68 ± 0.04	0.04 ± 0.01
EPMA	56.8 ± 1.0	4.4 ± 1.0	12.4 ± 0.3	0.66 ± 0.02	0.07 ± 0.02
$Th_{1.8}U_{0.2}(PO_4)_2(HPO_4)\cdot H_2O$					
Calc.	54.3	6.2	12.1	0.67	0.1
PIXE	59.2 ± 3.0	4.3 ± 0.2	11.9 ± 0.6	0.69 ± 0.04	0.08 ± 0.02
EPMA	56.3 ± 1.3	5.4 ± 1.2	12.1 ± 0.2	0.68 ± 0.02	0.08 ± 0.02
$ThU(PO_4)_2(HPO_4)\cdot H_2O$					
Calc.	30.0	30.7	12.0	0.67	0.5
PIXE	31.9 ± 1.6	31.7 ± 1.6	12.0 ± 0.6	0.65 ± 0.04	0.50 ± 0.03
EPMA	30.7 ± 0.8	30.9 ± 0.9	12.2 ± 0.1	0.67 ± 0.01	0.49 ± 0.01
$Th_{0.8}U_{1.2}(PO_4)_2(HPO_4)\cdot H_2O$					
Calc.	23.9	36.8	12.0	0.67	0.6
PIXE	27.6 ± 1.4	36.0 ± 1.8	11.9 ± 0.6	0.65 ± 0.04	0.56 ± 0.03
EPMA	26.3 ± 3.9	35.8 ± 4.2	12.0 ± 0.4	0.68 ± 0.04	0.57 ± 0.06
$Th_{0.4}U_{1.6}(PO_4)_2(HPO_4)\cdot H_2O$					
Calc.	11.9	49.0	12.0	0.67	0.8
PIXE	13.8 ± 0.7	50.4 ± 2.5	11.6 ± 0.6	0.67 ± 0.04	0.78 ± 0.04
EPMA	10.5 ± 0.9	51.7 ± 0.9	11.9 ± 0.3	0.68 ± 0.02	0.83 ± 0.01
$Th_{0.2}U_{1.8}(PO_4)_2(HPO_4)\cdot H_2O$					
Calc.	6.0	55.0	11.9	0.67	0.9
PIXE	6.5 ± 0.3	57.5 ± 2.9	11.8 ± 0.6	0.66 ± 0.04	0.90 ± 0.05
EPMA	5.0 ± 1.1	57.5 ± 1.3	11.8 ± 0.2	0.69 ± 0.02	0.92 ± 0.02
$U_2(PO_4)_2(HPO_4)\cdot H_2O$					
Calc.	0	61.0	11.9	0.67	1
PIXE	–	64.1 ± 3.2	11.7 ± 0.6	0.67 ± 0.04	–
EPMA	–	63.1 ± 0.6	11.5 ± 0.3	0.71 ± 0.03	–

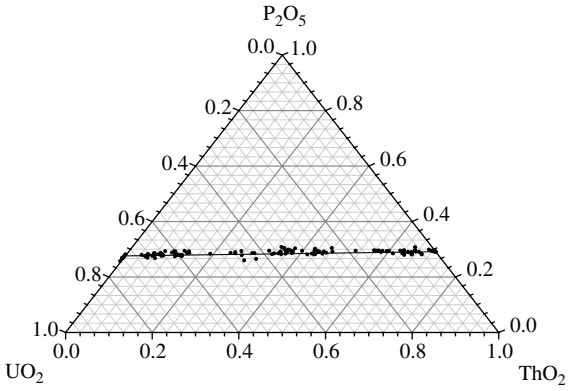

Fig. 1. Representation of the electron probe microanalysis results obtained for TUPHPH solid solutions in the ternary system ThO_2–UO_2–P_2O_5 (calculated in wt%).

in observations of polished sections (Fig. 4(e) and (f)). These aggregates appear as balls with an empty core and radial organization of the micrometric crystals generating a spherulitic texture. This morphology could result from the dehydration of the gelatinous phase initially formed during the synthesis. These structures are more easily formed when the thorium substitution rate is close to 2. Similar morphologies are also observed on the compounds heated at 400 °C under inert atmosphere (not illustrated in this work).

3.1.4. Transmission electron microscopy (TEM)

Several micrographs of TUPHPH (Fig. 5) were collected using different TEM modes (bright field (Fig. 5(a) and (b)), dark field (Fig. 5(c) and (d)), lattice fringes (Fig. 5(e)) and selected area diffraction (Fig. 5(f))). Bright field observations of the powder confirmed the existence of aggregates constituted by small flat paral-

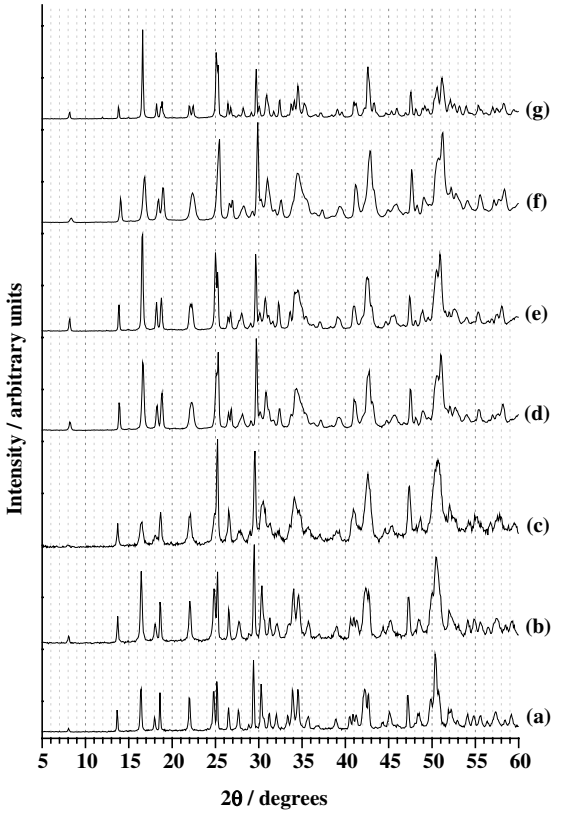

Fig. 2. XRD diagrams of $Th_{2-x/2}U_{x/2}(PO_4)_2(HPO_4)\cdot H_2O$ prepared at 150 °C (1 week) with $x = 0$ (a); 0.5 (b); 2.0 (c); 2.5 (d); 3.0 (e); 3.5 (f) and 4.0 (g).

lelipedic crystals of about 1 μm by 100 nm. In the SAD mode, this morphology led to crystals lying preferentially along one face (corresponding to (a,b)). The crystallization state and the size distribution of the coherent domains were then verified using dark field mode for several azimutal positions of the electron beam (90° and 180° or 0° and 90°). The samples are perfectly crystallized since the particles appeared lightened for the 90° position (Fig. 5(c)) and darkened for 180° (Fig. 5(d)). Lattice fringes micrographies also confirmed the good crystallization state of the sample since the fringes (Fig. 5(e)) reach the surface of the grains. Finally, no halo, characteristic of amorphous phases, was observed in any selected area diffraction pictures (from Fig. 5(f)).

3.2. Behavior of TUPHPH versus heat temperature

3.2.1. XRD study

As already described, previous studies were already dedicated to the thermal behavior of TPHPH [22]. From NMR (^1H and ^{31}P), IR and Raman spectroscopies, the solid was found to be fully dehydrated after heating between 170 °C and 200 °C, leading to the proposed formula $Th_2(PO_4)_2(HPO_4)$ (TPHP). Heated between 200 °C and 270 °C, this solid transforms into α-$Th_4(PO_4)_4P_2O_7$ (α-TPD) by condensation of hydrogenphosphate groups into diphosphate entities while the XRD pattern remains almost unchanged (only a small contraction of the unit cell parameters is observed). Above 900–950 °C, pure and single phase β-TPD is obtained [22].

Table 2
Unit cell parameters and volume of TUPHPH solid solutions (θ = 150–160 °C, 1 week)

	$x = 0$	$x = 0.16$	$x = 0.32$	$x = 0.50$	$x = 1.00$
a/Å	6.695(1)	6.690(2)	6.685(2)	6.683(2)	6.669(2)
b/Å	7.024(1)	7.026(2)	7.023(2)	7.018(2)	7.007(2)
c/Å	11.205(3)	11.194(6)	11.194(4)	11.196(4)	11.164(5)
β/Å	107.35	107.31(3)	107.36(4)	107.31	107.32
V/Å^3	503.0 ± 1.0	502.3 ± 1.0	501.6 ± 1.0	501.4 ± 1.0	498.0 ± 1.0
	$x = 1.50$	$x = 1.60$	$x = 2.00$	$x = 2.24$	$x = 2.50$
a/Å	6.658(2)	6.653(2)	6.642(4)	6.630(4)	6.634(13)
b/Å	7.001(2)	6.999(3)	6.992(4)	7.001(7)	6.984(10)
c/Å	11.148(3)	11.142(3)	11.122(11)	11.112(6)	11.088(23)
β/Å	107.36	107.31	107.36	107.31	107.40(4)
V/Å^3	496.0 ± 1.0	495.3 ± 1.0	493.0 ± 1.0	492.4 ± 1.0	490.2 ± 1.0
	$x = 3.12$	$x = 3.50$	$x = 4.00$		
a/Å	6.614(5)	6.609(9)	6.608(4)		
b/Å	6.981(7)	6.980(13)	6.952(6)		
c/Å	11.078(10)	11.050(20)	11.058(11)		
β/Å	107.32(8)	107.34(5)	107.34		
V/Å^3	488.4 ± 1.0	486.7 ± 1.0	484.9 ± 1.0		

Table 3
Variation of unit cell parameters and volume of TUPHPH solid solutions versus the substitution ratio x

a/Å	6.693(2)–0.024(1) x_U
b/Å	7.027(2)–0.017(1) x_U
c/Å	11.206(2)–0.0392(13) x_U
V/Å^3	503.07(±0.21)–4.73(±0.10) x_U

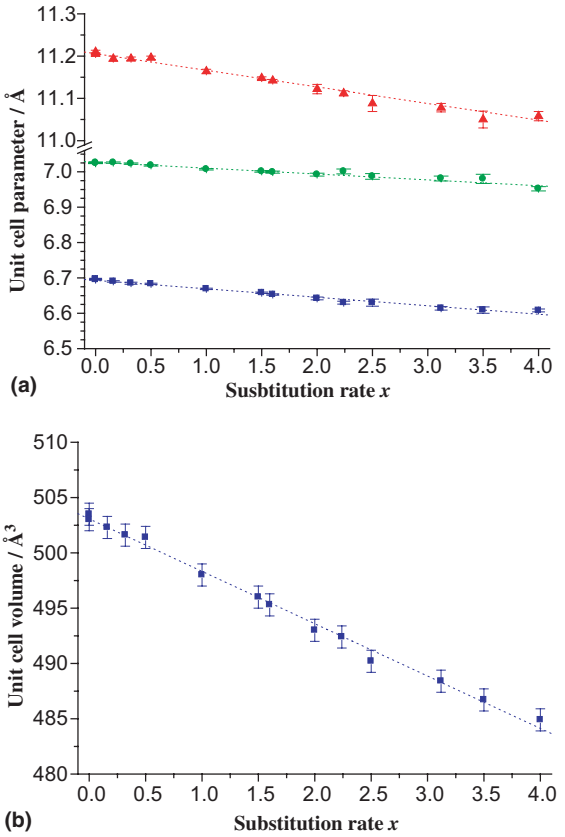

Fig. 3. Variation of the unit cell parameters of $Th_{2-x/2}U_{x/2}(PO_4)_2(HPO_4)\cdot H_2O$ (a), a (■); b (●) and c (▲); and volume (b) versus the x value.

We already mentioned that the preparation of β-TUPD solid solutions was not possible for $x \geqslant 3.0$ by any of the chemical routes already described [23]. Moreover, it was also difficult to get homogeneous and single phase samples due to the oxidation of tetravalent uranium for low uranium contents, especially through wet chemistry routes, or to the low reactivity of the reagents (for dry chemistry methods) [23].

In this study, we examined the thermal behavior of several TUPHPH samples for $x \leqslant 3.0$. The XRD patterns of TUPHPH ($x = 0.4$) followed from 25 °C to 1175 °C (Fig. 6(a)) showed that solid solutions of TUPHPH (then α-TUPD for $\theta \geqslant 200$ °C) follow the same chemical scheme of reaction than that of TPHPH, but only for x values lower than 2.8. Indeed, for $x = 0.4$, the XRD diagram recorded at room temperature is kept up to 875 °C. Above this temperature, the apparition of additional diffraction lines indicates that α-TUPD (monoclinic) is transformed into β-TUPD (orthorhombic). This irreversible phase transition is complete at 950 °C while β-TUPD is stable up to 1300 °C. No additional diffraction line is found on the diagram excluding the presence of secondary phases such as α-MP_2O_7, $M_2(PO_4)(P_3O_{10})$ or $M_2O(PO_4)_2$ (M = Th and/or U).

The same study was devoted to solid solutions with $x > 2.8$. The variation of the XRD diagram of TUPHPH (with $x = 3.6$, Fig. 6(b)) versus temperature shows that this solid is stable up to 600 °C. Above this temperature, it is transformed into a mixture of β-TUPD, α-$Th_{1-z}U_zP_2O_7$ and $U_{2-w}Th_wO(PO_4)_2$ instead of leading to pure β-TUPD solid solution which is consistent with literature [18,19,23].

3.2.2. Spectroscopic study

The transformation of the solids was also followed by the means of IR and Raman techniques (Figs. 7 and 8). A proposed assignment of the absorption bands is reported in Table 4 for TUPHPH and for α-TUPD.

At room temperature, the IR spectrum is consistent with that of TPHPH. The solids are hydrated since the water absorption bands are observed at 3600 cm^{-1} (ν_{OH}) and around 1610–1630 cm^{-1} (δ_{H_2O}). The band pointed out between 930 and 970 cm^{-1} could be assigned either to ν_s(P–O), ν_{as}(P–O–P) and $\delta_{out\ of\ plane}$(P–O–(H)) vibrations. In the same way, the band located near 1250 cm^{-1} could be associated to $\delta_{in\ the\ plane}$(P–O–(H)) and/or to water molecules adsorbed on phosphate layers. The existence of P–O–P groups was excluded in pure TPHPH [22].

Only weak differences are found after heating the samples between 250 °C and 950 °C since all the vibration modes (ν_{as}, ν_s, δ_{as} and δ_s) of the P–O edge of the PO_4 group [32] are observed. Nevertheless, a single additional absorption band (pointed by an arrow in the graph) appears at 770 cm^{-1} (IR) and 776 cm^{-1} (Raman) above 250 °C showing the transformation of TUPHPH into α-TUPD. This band, assigned to the symmetric stretching mode of the P–O–P bridge of the P_2O_7 group results from the condensation of hydrogenphosphate groups into diphosphate entities as it is observed in several compounds [33–35]. It is not modified until α-TUPD is transformed into β-TUPD.

Some significant modifications of the HT-Raman spectra occur between 25 °C and 300 °C (Fig. 8(a)). The ν_s(P–O–P) (770–780 cm^1) vibration mode of P_2O_7 is not present on the Raman spectrum recorded at room temperature but weakly appears above 200 °C. Moreover, it becomes progressively more intense at 250 °C,

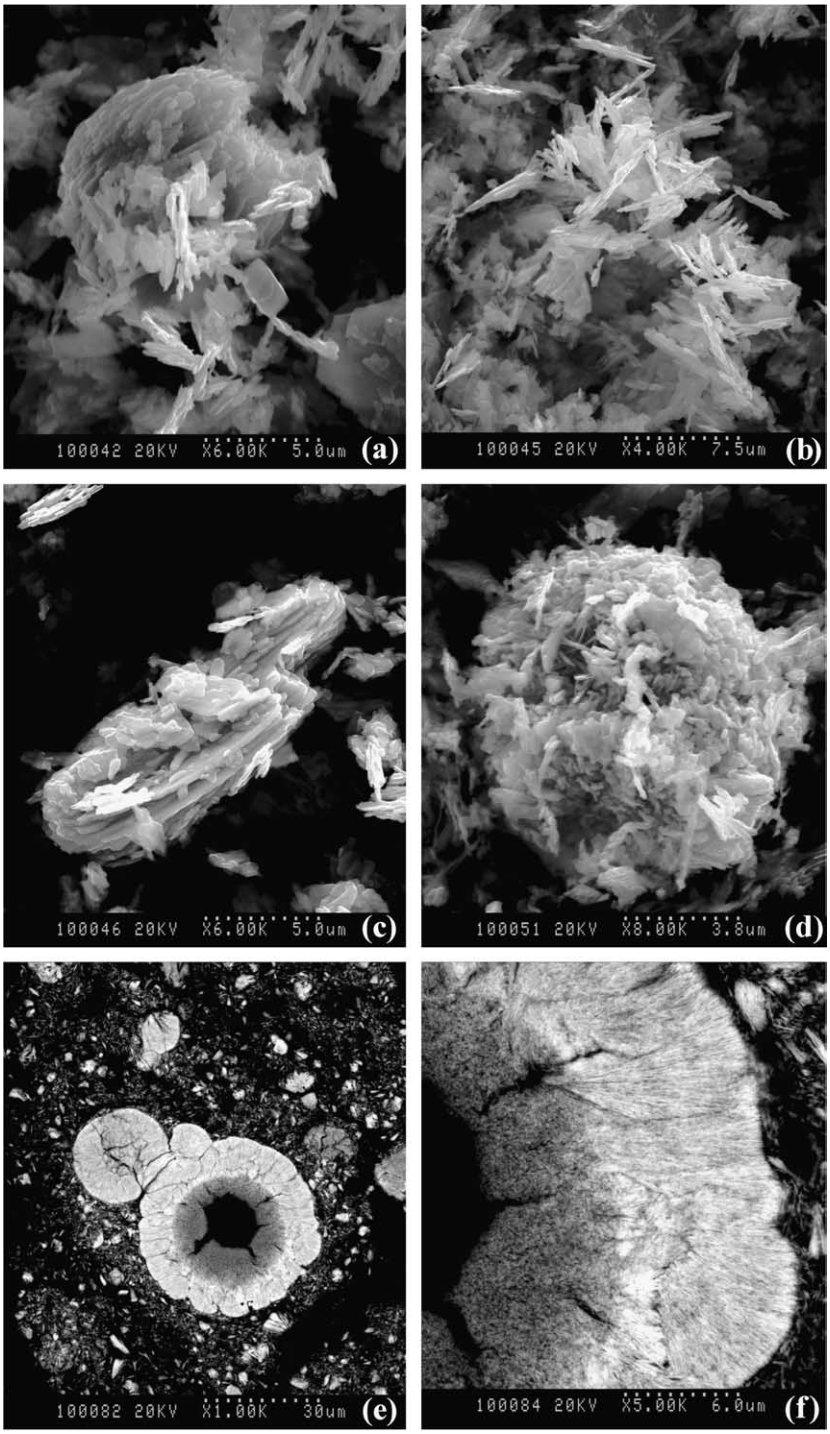

Fig. 4. Scanning electron micrographies of powdered $Th_{2-x/2}U_{x/2}(PO_4)_2(HPO_4)\cdot H_2O$ with $x = 0.4$ (a)–(c) and $x = 3.2$ (d) and on polished section with $x = 3.2$ (e)–(f).

which indicates that the transformation of HPO_4 entities into P_2O_7 groups is progressive between 200 °C and 250 °C. After heating at 800 °C, the ν_s(P–O–P) band is still visible on the spectrum (Fig. 8(b)). Above 1000 °C, this band is split in two components (at 705 and 741 cm^{-1}) corresponding to β-TUPD [14]. The spectra

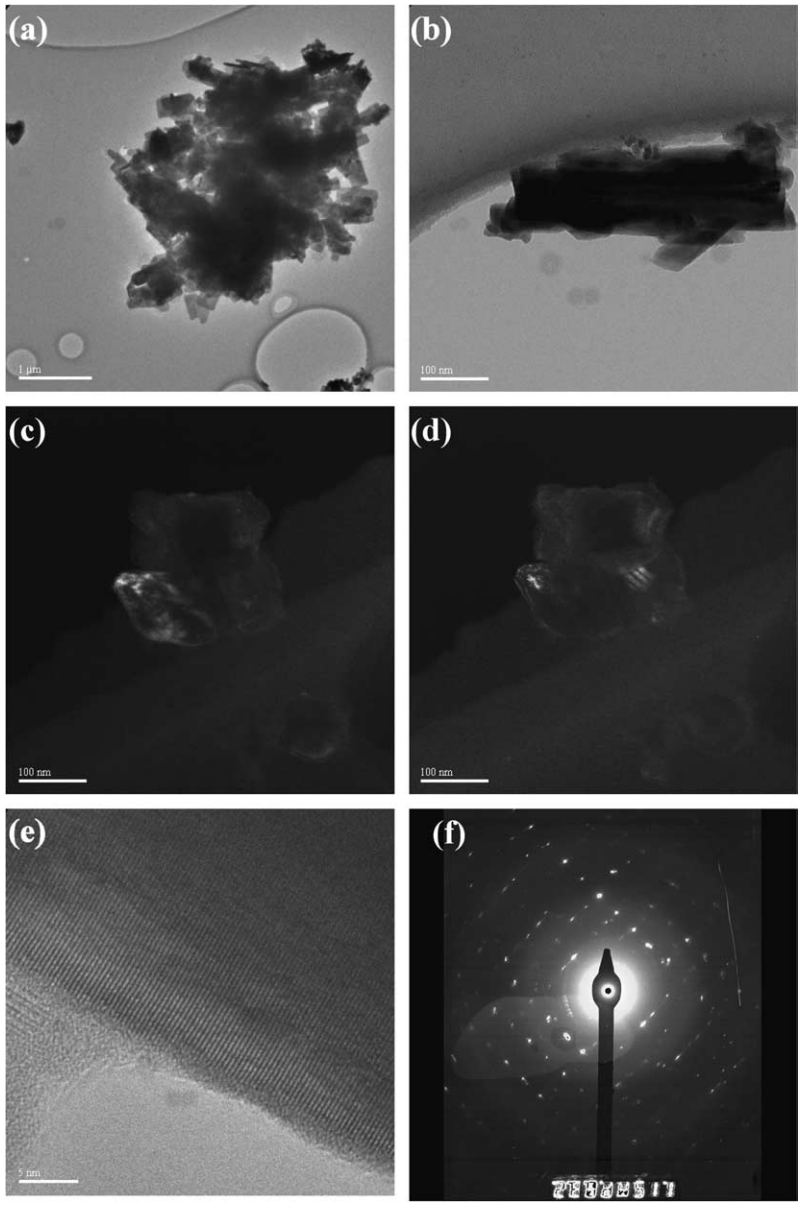

Fig. 5. Transmission electron micrographies of powdered TUPHPH ($x = 1.6$): bright field (a)–(b), dark field (c)–(d), lattice fringes (e) and selected area diffraction (f).

also exhibited a weak band located at 850 cm^{-1}, which could suggest the presence of small amounts of uranyl molecular ion (v_1(U = O) vibration) [36], probably included in minor phases at the surface of the samples. However, this band is usually very intense in uranyl-bearing compounds and XPS experiments performed on TUPHPH did not reveal significant amounts of uranium (VI) at the surface of the samples.

The solid is always found to be hydrated up to 950 °C, which is quite surprising considering DTA and TGA experiments (see following section). In fact, the compound is completely dehydrated when heating above 400 °C. Nevertheless, it exhibits a strong hygroscopic behavior during cooling, even under argon atmosphere (≈1000 ppm H_2O). This behavior was also confirmed for samples left in air for several days.

3.2.3. TG and DT analyses

In order to confirm the general scheme of reactions occurring from TUPHPH to β-TUPD, the behavior of TUPHPH ($x = 1.6$) was followed from room temperature to 1200 °C through TGA and DTA experiments

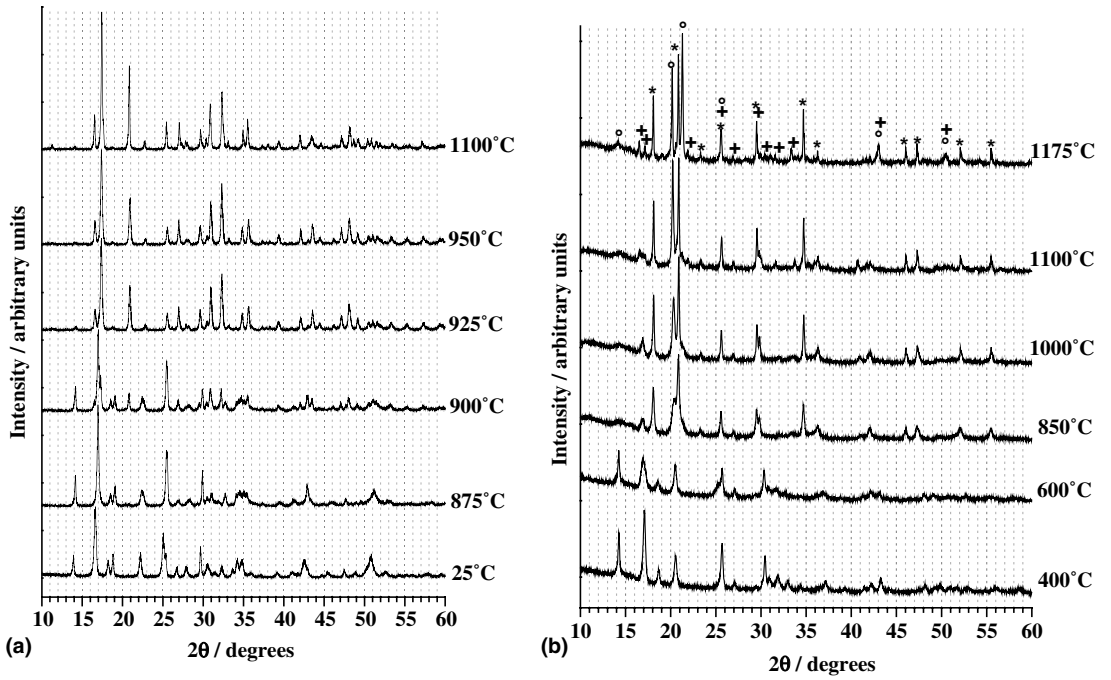

Fig. 6. Variation of the XRD diagrams of TUPHPH versus the heat temperature for $x = 0.4$ (a) and for $x = 3.6$ (b). Diffraction lines of β-$Th_{4-y}U_yP_6O_{23}$ (+), $U_{2-w}Th_wO(PO_4)_2$ (○) and α-$Th_{1-z}U_zP_2O_7$ (*).

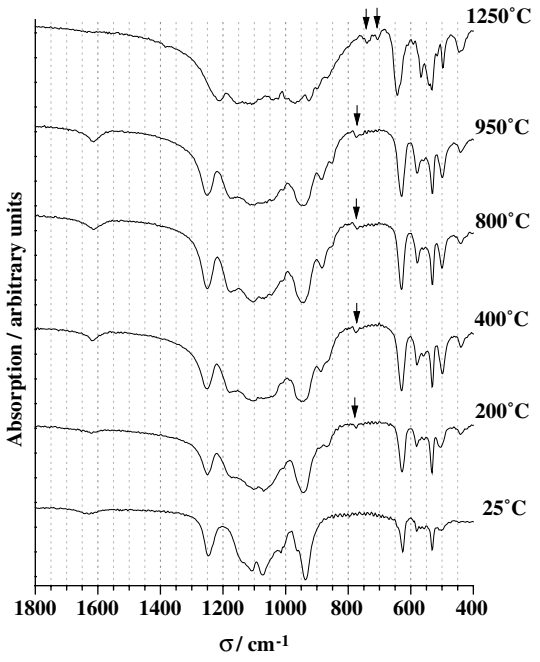

Fig. 7. Variation of IR spectra of TUPHPH solid solution ($x = 0.4$) versus heat temperature. The black arrows point out the ν_s(P–O–P) band characteristic of P_2O_7.

(Fig. 9, heating and cooling rates of 5 °C min^{-1}). The TGA curve exhibits three parts, from room temperature to 200 °C, from 200 °C to 300 °C and finally from 300 °C to 1200 °C. The maximal weight loss is achieved between room temperature and 300 °C and is correlated to two endothermic peaks. The first one, centered at 190 °C (−2.8 wt%) corresponds to the loss of $n = 1.2$ water molecules per unit formula $Th_{2-x/2}U_{x/2}(PO_4)_2(HPO_4)\cdot n\text{-}H_2O$. The second one is observed between 200 °C and 300 °C (centered at about 250 °C, −1.0 wt%) and corresponds to the loss of 0.45 additional water molecule per unit formula, due to the formation of P_2O_7 entities from HPO_4 groups (calculated additional weight loss: −1.1 wt%). α-TUPD (α-$Th_{4-x}U_x(PO_4)_4P_2O_7$) is thus formed from $Th_{2-x/2}U_{x/2}(PO_4)_2(HPO_4)\cdot H_2O$ above 200–300 °C.

A weak exothermic peak appears on DTA curve at 950 °C without any significant weight loss. This peak can be assigned to the transformation of α-TUPD into β-TUPD. A similar observation was reported for the transformation of dehydrated rhabdophane $LnPO_4$ (Ln = La–Dy, hexagonal system) into the $LnPO_4$ monazite (monoclinic system) [37]. Consequently, the following scheme of preparation of β-TUPD solid solutions from TUPHPH can be proposed:

$$2Th_{2-x/2}U_{x/2}(PO_4)_2(HPO_4)\cdot H_2O \xrightarrow{170\ ^\circ C\leqslant\theta\leqslant 200\ ^\circ C} 2Th_{2-x/2}U_{x/2}(PO_4)_2(HPO_4) + 2H_2O\uparrow \quad (1)$$

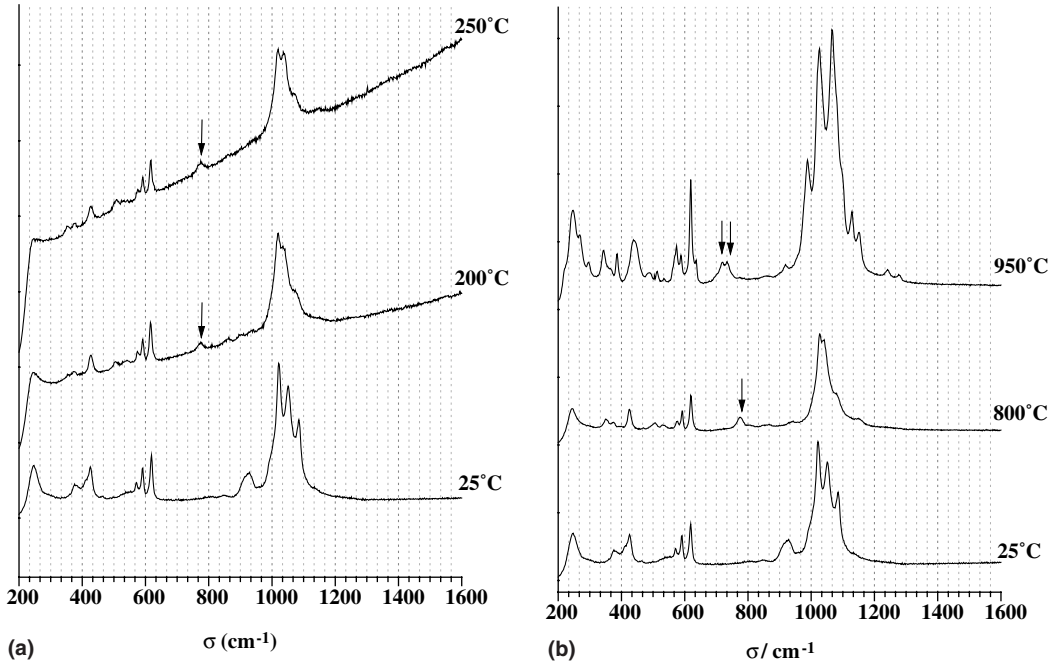

Fig. 8. HT-Raman spectra of TUPHPH ($x = 1.6$) versus the heat temperature (a) and Raman spectra versus heat temperature (b). The black arrows point out the ν_s(P–O–P) band characteristic of P_2O_7 entities.

Table 4
Assignment of the bands observed in the IR and Raman spectra of TUPHPH and of α-TUPD solid solutions (in cm^{-1})

	δ_s(P–O)	δ_{as}(P–O)	ν_s(P–O–P)	ν_{as}(P–O–P)	ν_s(P–O)	δ_{op}(P–O–(H))	ν_{as}(P–O)	δ_{ip}(P–O–(H))
RAMAN								
TUPHPH	375–430	570–620	–	–	925	925	1020–1085	N.O.[a]
α-TUPD[b]	350–425	500–620	776	945	N.O.[a]	–	1025–1145	N.O.[a]
IR								
TUPHPH	N.O.	500–650	–	<---------- 930-970 ---------->			1000–1150	1250
α-TUPD[b]	440	500–650	770	<---------- 890-970 ---------->			1000–1200	1252

[a] N.O.: not observed.
[b] Spectra recorded on samples previously heated between 200 °C and 950 °C.

$$2Th_{2-x/2}U_{x/2}(PO_4)_2(HPO_4) \xrightarrow{200\ ^\circ C \leqslant \theta \leqslant 300\ ^\circ C} \alpha - Th_{4-x}U_x(PO_4)_4P_2O_7\ (\text{monoclinic}) + H_2O\uparrow \quad (2)$$

followed by the irreversible phase-transition:

$$\alpha - Th_{4-x}U_x(PO_4)_4P_2O_7\ (\text{monoclinic}) \xrightarrow{\theta \approx 900-950\ ^\circ C} \beta - Th_{4-x}U_x(PO_4)_4P_2O_7(\text{orthorhombic}) \quad (3)$$

No significant decomposition of β-TUPD was observed up to 1300 °C.

3.2.4. Study of the samples homogeneity

In order to evidence the main advantages of this new chemical route involving TUPHPH as a precursor, i.e. the significant improvement of the chemical homogeneity of the β-TUPD samples prepared via the 'precipitation' route especially in terms of the distribution of actinides, a statistical survey of EPMA analyses was carried out on β-$Th_{2.4}U_{1.6}(PO_4)_4P_2O_7$ samples prepared by both methods (through direct evaporation of the mixture or via the initial precipitation of TUPHPH). For both powders, 50 analyses were performed and the variations of the U/(U + Th) mole ratio were carefully examined (Fig. 10). The homogeneity of the samples is significantly improved when using the 'precipitation' process (average: 0.32 ± 0.03 (σ), mainly spread from 0.27 to 0.39) instead of the 'direct evaporation' process (two main populations, average: 0.41 ± 0.05 (σ), mainly

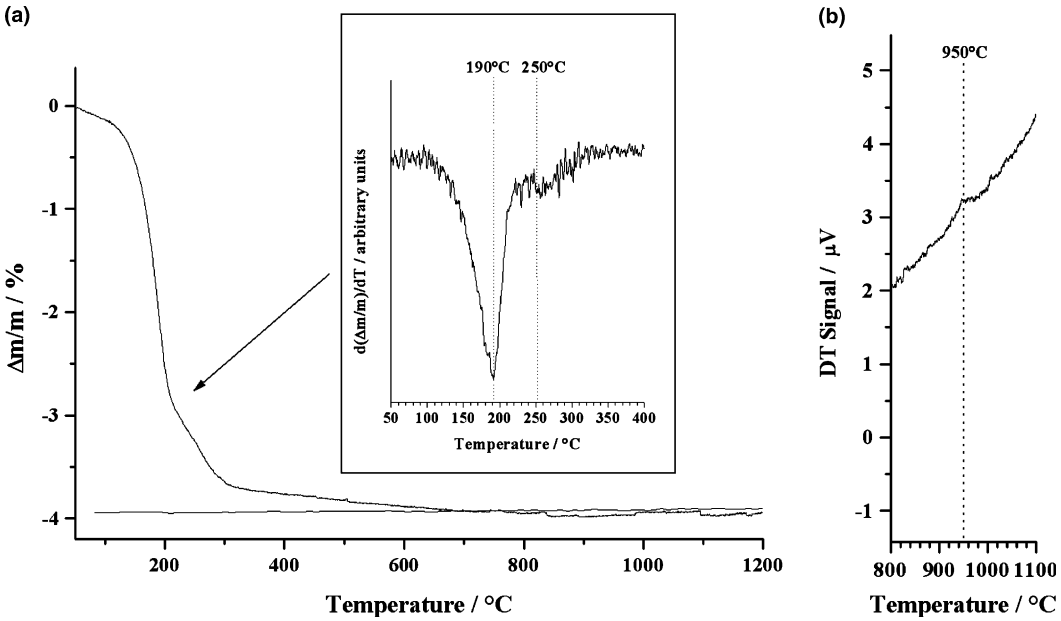

Fig. 9. TG (a) and DT (b) analyses of $Th_{1.2}U_{0.8}(PO_4)_2(HPO_4)\cdot H_2O$.

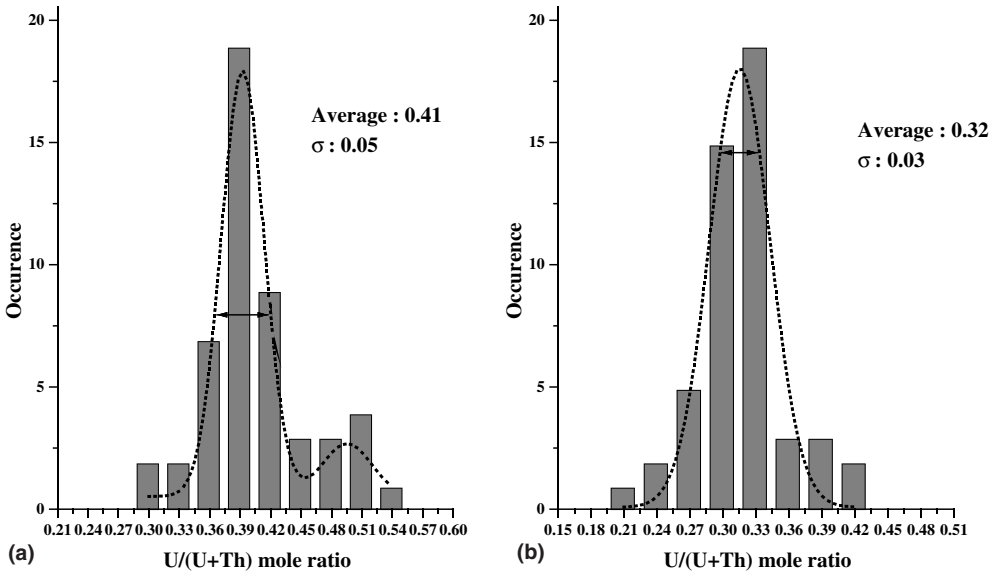

Fig. 10. Statistical variations of the U/(U + Th) mole ratios in β-TUPD solid solutions ($x = 1.6$) prepared through 'direct evaporation' (a) or via the 'precipitation' process (b). Gap-type is materialized by a black arrow.

spread from 0.33 to 0.51). This observation can be correlated to the narrower dispersion of the data gathered in the ThO_2–UO_2–P_2O_5 ternary diagrams (data reported in wt%) for samples prepared via the precipitation process compared to that obtained through direct evaporation (Fig. 11). The homogeneity is even better on sintered samples [38] which could ensure the high chemical durability of β-TUPD samples during leaching tests. However, the 'precipitation' process leads to a partial oxidation of tetravalent uranium (about 5–10%) into uranyl which is not incorporated in the precursor (uranyl is not precipitated in these experimental conditions). That explains the difference between the U/(U + Th) mole ratio determined for this route (0.32) compared

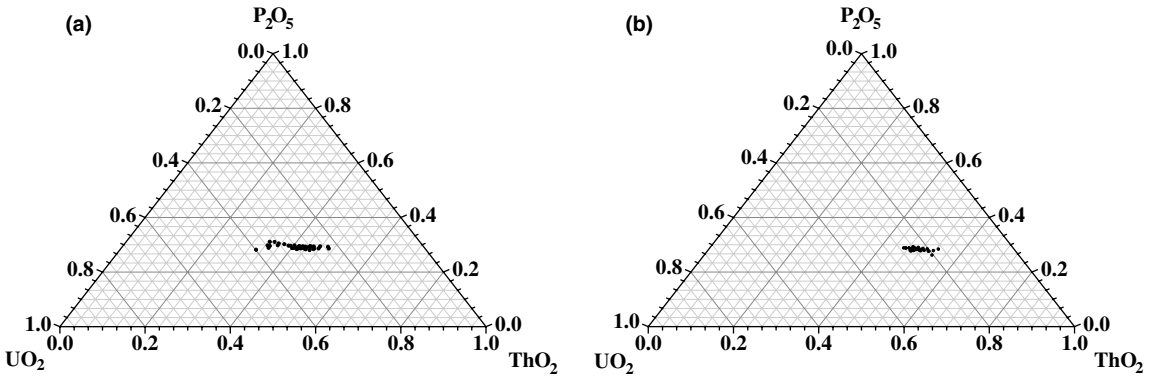

Fig. 11. Representation of the results of electron probe microanalysis of β-TUPD solid solutions ($x = 1.6$) prepared through 'direct evaporation' (a) or via the 'precipitation' process (b) in the ternary system ThO_2–UO_2–P_2O_5 (calculated in wt%).

to that expected (0.40). In conclusion, this method appears better as far as the homogeneity is significantly improved even though the uranium uptake is not quantitative. This latter point could be partially resolved by making the precipitation in anoxic conditions.

4. Conclusion

Well crystallized thorium and uranium phosphates were synthesized for various compositions through a wet chemistry method in closed containers. PIXE and EPMA experiments confirmed that the samples were homogeneous and single phase. These products were identified as the thorium–uranium (IV) phosphate–hydrogenphosphate hydrate (TUPHPH), $Th_{2-x/2}U_{x/2}(PO_4)_2(HPO_4) \cdot H_2O$, stable between 150 °C and 200 °C. Complete solid solutions were found between both TPHPH and UPHPH end-members ; the variations of the corresponding unit cell parameters remains weak ($\Delta V/V \approx 4\%$). From IR or Raman spectroscopy, on the one hand, and TGA and DTA results on the other hand, a new low-temperature variety of the thorium–uranium (IV) phosphate–diphosphate solid solutions (α-$Th_{4-x}U_x(PO_4)_4P_2O_7$, monoclinic system) was identified after heating between 200 °C and 900–950 °C. The presence of P_2O_7 groups was clearly established for samples heated above 200 °C.

By this new chemical route, well crystallized, pure and homogeneous β-TUPD solid solutions were prepared above 950 °C under inert atmosphere, in all the domain of composition ranging from pure TPHPH to TUPHPH ($x = 2.8$). Above this x value, polyphase systems composed by $U_{2-w}Th_wO(PO_4)_2$, α-$Th_{1-z}U_zP_2O_7$ and β-TUPD are obtained. The preparation of dense pellets of β-TUPD solid solutions from TUPHPH precursors was also performed with success (relative densities of 95–98% of the value calculated from XRD data) [38]. Finally, this efficient precipitation of tetravalent actinides could be applied for the decontamination of radioactive liquid waste containing α-emitters. In this aim, the incorporation of other tetravalent actinides (Np, Pu) in the TPHPH and in the α-TPD structures was also examined [39].

Acknowledgments

The authors would like to thank Lionel Aranda, Johann Ravaux, Jean-Paul Emeraux and Alain Kohler from the LCSM and Thérèse Lhomme from the CREGU of the University Henri Poincaré – Nancy (France) for performing EPMA, XRD, Raman, TGA/DTA experiments and the SEM observations. They would also like to thank Gérard Lagarde from IPNO for performing PIXE experiments. Authors are also very grateful to Professor Michel Quarton from University Pierre and Marie Curie – Paris-VI (France) for understanding in the XRD experiments and to Professor Joël Emery of the University of Le Mans (France) for the NMR studies on TPHPH and α-TPD. The authors thank Professor J. Rubén García from University of Oviedo (Spain) for making the determination of the structure of TPHPH.

References

[1] J. Carpena, F. Audubert, D. Bernache, L. Boyer, B. Donazzon, J.L. Lacout, N. Senamaud, in: I.G. McKinley, C. McCombie (Eds.), Scientific Basis for Nuclear Waste Management XXI, vol. 506, 1998, p. 543.
[2] R. Bros, J. Carpena, V. Sere, A. Beltritti, Radiochim. Acta 74 (1996) 277.
[3] L.A. Boatner, B.C. Sales, in: W. Lutze, R.C. Ewing (Eds.), Radioactive Waste Forms for the Future, North-Holland Physics Publishing, Amsterdam, 1998, p. 495.

[4] J.M. Montel, J.L. Devidal, D. Avignant, Chem. Geol. 191 (2002) 89.
[5] R. Podor, M. Cuney, Am. Miner. 82 (1997) 765.
[6] R. Podor, M. Cuney, C. Nguyen Trung, Am. Miner. 80 (1995) 1261.
[7] A. Meldrum, L.A. Boatner, W.J. Weber, R.C. Ewing, Geochim. Cosmochim. Acta 62 (1998) 2509.
[8] M.M. Abraham, L.A. Boatner, T.C. Quinby, D.K. Thomas, M. Rappaz, in: Radioactive Waste Management, vol. 1, 1980, p. 181.
[9] O. Terra, N. Clavier, N. Dacheux, R. Podor, New J. Chem. 27 (2003) 957.
[10] H.T. Hawkins, B.E. Scheetz, G.D. Guthrie, Mater. Res. Soc Symp. Proc. 465 (1996) 387.
[11] H.T. Hawkins, D.R. Spearing, G.D. Guthrie, Chem. Mater. 11 (1999) 2851.
[12] S. Nakayama, K. Itoh, J. Eur. Ceram. Soc. 23 (2003) 1047.
[13] A.I. Orlova, Y.F. Volkov, R.F. Melkaya, L.Y. Masterova, I.A. Kulikov, V.A. Alferov, Radiokhimiya 36 (1994) 322.
[14] P. Benard, V. Brandel, N. Dacheux, S. Jaulmes, S. Launay, C. Lindecker, M. Genet, D. Louër, M. Quarton, Chem. Mater. 8 (1996) 181.
[15] N. Dacheux, N. Clavier, P. Le Coustumer, R. Podor, in: P. Vicenzini (Ed.), Proceeding of the 10th International Ceramic Congress, vol. 33, Faenza, Italy, 2002, p. 201.
[16] N. Clavier, N. Dacheux, O. Terra, P. Le Coustumer, R. Podor, in: P. Vicenzini (Ed.), Proceeding of the 10th International Ceramic Congress, vol. 33, Faenza, Italy, 2002, p. 209.
[17] V. Brandel, N. Dacheux, M. Genet, Radiokhim. 43 (2001) 16.
[18] N. Dacheux, R. Podor, B. Chassigneux, V. Brandel, M. Genet, J. Alloys Comp. 271 (1998) 236.
[19] N. Dacheux, R. Podor, V. Brandel, M. Genet, J. Nucl. Mater. 252 (1998) 179.
[20] N. Dacheux, A.C. Thomas, V. Brandel, M. Genet, J. Nucl. Mater. 257 (1998) 108.
[21] A.C. Robisson, N. Dacheux, J. Aupiais, J. Nucl. Mater. 306 (2002) 134.
[22] N. Dacheux, N. Clavier, G. Wallez, V. Brandel, J. Emery, M. Quarton, M. Genet, Chem. Mater., submitted for publication.
[23] N. Dacheux, V. Brandel, M. Genet, K. Bak, C. Berthier, New J. Chem. 20 (1996) 301.
[24] N. Dacheux, B. Chassigneux, V. Brandel, P. Le Coustumer, M. Genet, G. Cizeron, Chem. Mater. 14 (2002) 2953.
[25] A.C. Thomas, N. Dacheux, P. Le Coustumer, V. Brandel, M. Genet, J. Nucl. Mater. 281 (2000) 91.
[26] A.C. Thomas, N. Dacheux, P. Le Coustumer, V. Brandel, M. Genet, J. Nucl. Mater. 295 (2001) 249.
[27] E.H. Oelkers, F. Poitrasson, Chem. Geol. 191 (2002) 73.
[28] V. Brandel, N. Dacheux, M. Genet, J. Solid State Chem. 159 (2001) 139.
[29] Diffrac-AT V 3.0 Software package, Socabim, France.
[30] M. Evain,U-Fit Program, Institut des Matériaux de Nantes, France, 1992.
[31] M.A. Salvadó, P. Pertierra, A.I. Bortun, C. Trabajo, J.R. García, N. Clavier, N. Dacheux, Chem. Mater., submitted for publication.
[32] A. Rulmont, R. Cahay, M. Liegeois-Duyckaerts, P. Tarte, Eur. J. Solid State Inorg. Chem. 28 (1991) 207.
[33] J. Chen, M. Liu, H. Pan, S. Lin, X. Xin, J. Solid State Chem. 159 (2001) 130.
[34] R.K. Chiang, C.C. Huang, C.R. Lin, C.S. Wur, J. Solid State Chem. 156 (2001) 242.
[35] M. Suàrez, L.M. Barcina, R. Llavona, J. Rodríguez, J. Mol. Struct. 470 (1998) 105.
[36] J.R. Bartlett, R.P. Cooney, J. Mol. Struct. 193 (1989) 295.
[37] R.G. Jonasson, E.R. Vance, Thermochim. Acta 108 (1986) 65.
[38] N. Clavier, N. Dacheux, P. Martinez, E. Du Fou de Kerdaniel, R. Podor, L. Aranda, Chem. Mater. 16 (2004) 3357.
[39] J. Rousselle, in: Etude de la formation du phosphate-diphosphate de thorium (PDT) en milieu nitrique en vue d'une décontamination d'effluents de haute activité contenant des actinides, Thesis, University Paris-Sud-XI, IPNO-T-04.03, 2004.